Single Molecule Discrimination of Heteropolytungstates and Their Isomers in Solution with a Nanometer-Scale Pore

Jessica Ettedgui,*,[†,‡] John J. Kasianowicz,[†] and Arvind Balijepalli[†]

[†]Engineering Physics Division, Physical Measurement Laboratory, National Institute of Standards and Technology, Gaithersburg, Maryland 20899, United States

[‡]Department of Chemical Engineering, Columbia University, New York, New York 10027-6623, United States

Ⓢ *Supporting Information*

ABSTRACT: We report a new method to identify metallic nanoclusters (polyoxometalate structures) in solution at the single molecule limit using a nanometer-scale pore. The technique allows the measurement of polyoxometalates with over 2 orders of magnitude lower analyte concentration than conventional analytical chemistry tools. Furthermore, pH-dependent structural changes in phosphotungstic acid are measured with protein nanopores and validated with NMR. We further demonstrate that the method can also discriminate $[PW_9O_{34}]^{9-}$ structural isomers. The results suggest this technique can serve as a complementary approach to traditional methods.

Membrane-bound protein nanometer-scale pores have been used to detect, characterize and quantify ions,[1] RNA and DNA polynucleotides,[2] DNA damage,[3] polymers via gold nanoparticle-induced transport rate reduction,[4] synthetic polymers,[5] small molecule enantiomers,[6] anthrax toxins,[7] and unfolded proteins.[8] We demonstrate here that the nanopore formed by the bacterial protein exotoxin *Staphylococcus aureus* alpha hemolysin (αHL)[9] can also characterize anionic metal oxygen clusters, polyoxometalates (POMs), at the single molecule limit. Although POMs were discovered nearly two centuries ago,[10] they still attract considerable interest because of the breadth of their applications[11] in electrochemistry,[12] photochromism,[13] magnetism,[14] catalysis,[15] and materials science.[16] There has also been growing interest in the use of POMs for medical applications[11,17] because they selectively inhibit enzymatic activity, and they have antitumor,[18] antiviral,[11] and anticoagulant properties.[19] POMs exhibit diversity in size, charge, and shape. They are highly ordered clusters and can present isomeric forms, which can be used to tune their properties with controlled geometrical changes, such as the different location of a given atom (positional isomerism) or a rotation of a fragment of the molecule (rotational isomerism).[20] Tungsten polyoxometalates are stable in acidic aqueous solution, but degrade in a complex manner into a mixture of inorganic products when the pH is increased. This process is initiated by hydrolytic cleavage of the metal–oxygen (M–O) bonds, which triggers the loss of one or three MO_6 octahedral subunits,[21] giving rise to monovacant and trivacant species also called "*lacunary*" (or defect) derivatives (e.g., the Keggin-type polyanion).[22] In aqueous solutions, they are

subject to complete decomposition by OH^- ions (i.e., $PW_{12}O_{40}{}^{3-} + 23OH^- \rightarrow HPO_4{}^{2-} + 12WO_4{}^{2-} + 11H_2O$).[20]

We show here that the highly sensitive nanopore-based technique[23] permits the detection of subtle differences in POM structure elicited by pH changes and at nearly 2 orders of magnitude lower concentration than those required for NMR spectroscopy and other classical methods. Importantly, this approach also allows the discrimination of isomeric forms of $Na_8HPW_9O_{34}$ and complements traditional analytical chemistry techniques used to characterize POM structures.[20]

The experimental setup for single POM molecule measurements with an αHL nanopore is illustrated in Figure 1A: two
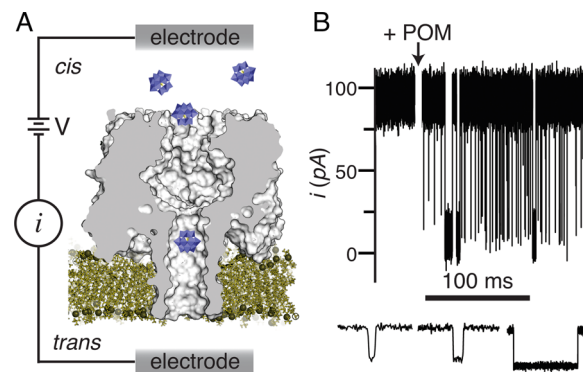
Figure 1. Detection of individual polyoxometalates (POMs) with a single nanometer-scale pore. (A) Schematic illustration of the method. A voltage (*V*) drives an ionic current through the pore (*i*), which is reduced by the entry of a single POM molecule. (B) Ionic current time series before and after the addition of highly negatively charged POM particles to the *cis* chamber (top) with *V* = 120 mV and an aqueous solution that contains 1M NaCl, 10 mM NaH_2PO_4, 5 μM 12-phosphotungstic acid at pH 5.5. Three typical single molecule current blockades (bottom). A negative applied potential drives anions from the *cis* to the *trans* compartment.

chambers filled with electrolyte solution (1 M NaCl, 10 mM NaH_2PO_4 at pH 5.5) are separated by a pore embedded in a 4 nm thick electrically insulating phospholipid membrane. An electrical potential *V* drives an ionic current *i*, due to Na^+ and Cl^- ions, through the pore. At *V* = 120 mV, the mean current $\langle i \rangle$ is (95 ± 3) pA (Figure 1B), and the spontaneous reversible partitioning of

individual POMs from the *cis* side of the pore causes well-defined transient current reductions. The characteristic residence times of an ionic current blockade, τ_{res} (time a given molecule spends in the pore) are of order 100 microsecond, $\approx 10^3$ fold longer than expected for a nanoparticle diffusing the length of the pore. The POM capture rate (rate at which molecules enter the pore) increased linearly with concentration (slope = 6.4 $\mu M^{-1}s^{-1}$, Supporting Information, SI1). Reversing the polarity of the potential prevented POM from entering the nanopore, as expected (SI2). Due to their intrinsically anionic character, POMs are likely associated with organic counter cations through electrostatic interactions. Therefore, the choice of pH buffer must be made judiciously to maintain the free POM concentration.[24]

At pH 5.5, 12-phosphotungstic acid (PTA, $H_3PW_{12}O_{40}$) decomposes primarily into the monovacant anion $[PW_{11}O_{39}]^{7-}$,[11,25] that can be detected by a nanopore. Specifically, the histogram of the blockade depths for $V = 120$ mV (Figure 2A, red diamonds) shows a major peak at $\approx 84\%$
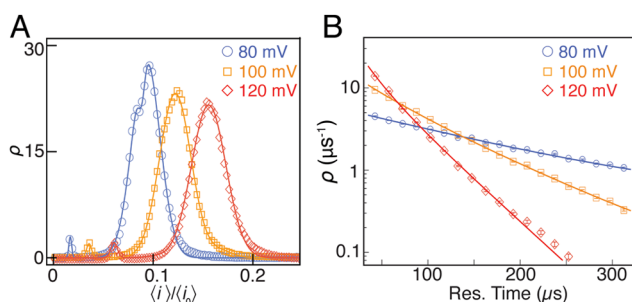
Figure 2. Voltage dependence of the probability density distributions (ρ) for POM-induced blockade depths and residence times for POMs in the nanopore. (A) The blockade depth ratio increases with increasing applied potential. (B) The residence time distributions show that, on average, the POMs spend less time in the pore with increasing voltage. The mean residence times of POMs in the pore (in μs), estimated by least-squares fit of exponential functions to the data are 249 (80 mV), 93 and 40 (100 mV), and 42, 20, and 12 (120 mV). The numbers of events obtained at these potentials are 175,000, 240,000, and 183,000, and data analysis is done with in-house software (MOSAIC).[28] The probability density is calculated by scaling the histograms (with bin size of 2.5×10^{-3} for the mean blockade depth ratios and 1.5 μs for the residence times) by the area under each curve.

current reduction (i.e., a current blockade ratio of $\langle i \rangle / \langle i_0 \rangle \approx 0.16$, where $\langle i \rangle$ and $\langle i_0 \rangle$ are the mean current values of the POM-occupied and fully open pore, respectively). There is also a minor peak at a deeper blockade state $\langle i \rangle / \langle i_0 \rangle \approx 0.06$. Because, the degree by which single nanoparticles reduce the nanopore current depends on the size, shape, and charge adsorbed on the molecule,[5a,26] the major and minor peaks might correspond to two different POM species.

The blockade depth ratios of the major and minor peaks decrease with decreasing applied potential (Figure 2A, $\langle i \rangle / \langle i_0 \rangle = 0.09 \pm 0.01$, 0.12 ± 0.01, and 0.16 ± 0.02 for $V = 80$, 100, and 120 mV, respectively for the major peak), as was observed for polyethylene glycol (PEG) molecules with αHL.[5a] Because the major peak at 80 mV has an additional component, we fitted the distribution of this peak to a two Gaussian mixture model (Figure 2A, blue solid line). A closer inspection of the blockade depth data shows that the widths of the major peaks increase with increasing potential (Figure 2A) and that the shoulder present at 80 mV can no longer be discriminated. Both observations suggest that

additional types of $[PW_{11}O_{39}]^{7-}$ partition into the pore at the higher voltages. This hypothesis is also consistent with the residence time data in Figure 2B. The distribution at $V = 80$ mV is well fitted by a single exponential function (Figure 2B, blue circles), which suggests the POM–pore interaction is described by a simple reversible binding reaction,[5] and the mean residence times for the two components are similar. However, the 100 and 120 mV residence time distribution data require 2 and 3 different exponentials, respectively (Figure 2B, orange squares and red diamonds). It is conceivable that as the applied potential is increased, POMs with different amounts of Na^+ bound to them (i.e., a different countercation stoichiometry in solution) can partition into the pore, which would cause the blockade depth peak width to increase and require additional time constants to fit the residence time data. Because the POM capture rate increases exponentially with the applied potential (SI3), there is likely an energy barrier to POM entry into the pore,[26a] which conceivably could control the POM species that can enter the pore based on their net charge.

The degradation products of PTA were measured with the nanopore in buffered aqueous solutions for pH values ranging from 5.5 to 9.0. The stock solutions ([POM] = 2 mM) were first measured with ^{31}P NMR prior to further dilution to 30 μM for the nanopore-based measurements. Over this range of pH, PTA decomposes into a monovacant anion $[PW_{11}O_{39}]^{7-}$[11,25] and a compound with a chemical shift of -1.5 ppm, consistent with $[P_2W_5O_{23}]^{6-}$.[25,29] Due to the low natural abundance of magnetically susceptible tungsten isotope and the low POM concentrations, the ^{183}W NMR spectrum could not be measured. It is generally accepted that the equilibria conditions, which control the formation of the more stable heteropolyanions, favor compounds with the highest heteroatom to tungsten ratios.[20] Following this line of reasoning, the formation of heteropoly-tungstate ions is more favorable because of the excess phosphate buffer present. The nanopore ionic current blockade ratio data in Figure 3A shows that the major and minor peaks in the probability density at pH 5.5 change as the pH is increased. A control experiment with a synthesized and highly purified sample of $[PW_{11}O_{39}]^{7-}$ (at pH 7.0) allowed the unambiguous assignment of the rightmost peak to $[PW_{11}O_{39}]^{7-}$, which suggests the leftmost peak corresponds to another species (likely $[P_2W_5O_{23}]^{6-}$).

As the pH increases from 5.5 to 7.5, the concentration of $[PW_{11}O_{39}]^{7-}$ decreases and that of $[P_2W_5O_{23}]^{6-}$ increases. The area under the peaks in Figure 3A shows that the loss of $[PW_{11}O_{39}]^{7-}$ exceeds the gain of $[P_2W_5O_{23}]^{6-}$, which suggests the concomitant formation of other degradation species that are not detected by the pore (i.e., free phosphate, $H_xPO_4^{-3+x}$ and tungstate, WO_4^{2-} ions). At pH 8, a third peak ($\langle i_3 \rangle / \langle i_0 \rangle = 0.24 \pm 0.03$) is apparent. Further increases in pH results in the complete loss of the two principal species as expected, due to their degradation into inorganic salts. Finally, the minor shifts in the nanopore blockade histogram peak values at different pH values may be due to the subtle fluctuations in the pore geometry[30] and to electrostatically induced changes in pore conductance due to the change in solution pH.[31]

The nanopore data were validated with ^{31}P NMR measurements of 2 mM stock POM solutions (Figure 3B). Peak assignment of tungstophosphate anions was initially performed using published NMR chemical shift values.[25] We further calibrated the peak assignments by repeating the ^{31}P NMR measurements with synthesized and purified samples of different tungstophosphate anions. At pH 7.5 (Figure 3B) and greater, the metal ion species were not visible in the ^{31}P NMR spectrum
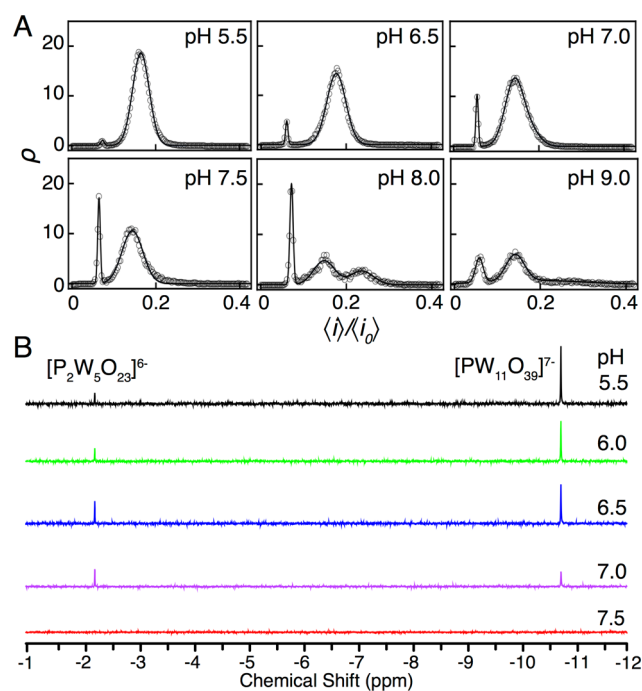
Figure 3. Effect of pH on 12-phosphotungstic acid (PTA) in solution monitored by a nanopore-based technology and NMR. (A) The probability density distributions (ρ) of PTA-induced ionic current blockade depths vary with pH at $V = 120$ mV. (B) ^{31}P NMR spectra (10% D_2O, 700 MHz) of stock solution 12-phosphotungstic acid (2 mM, $H_3PW_{12}O_{40}$) decomposition products in buffered aqueous solutions.

Figure 4. Discrimination of $Na_8HPW_9O_{34}$ isomers. (A) Schematic illustration of the $PW_{12}O_{40}$ Keggin ion and its Type A- and Type B-[PW_9O_{34}]$^{9-}$ isomers. (B) The isomers are distinguishable in solid state with IR. (C) Probability density of nanopore current single molecule blockade depth ratios for $Na_8HPW_9O_{34}$ Type A (blue squares) and Type B (red triangles) in solution with $V = 80$ mV. (D) Residence time distributions for $Na_8HPW_9O_{34}$ Type A and Type B in solution.

except for the signal of the free phosphate (SI4). In contrast, the nanopore's 70-fold higher sensitivity in analyte concentration allowed the detection of these and other species. Finally, it should be noted that the limit of detection for single molecules can be further improved by collecting data for longer times.

POMs exhibit a diversity of structure, obtained in some instances by the removal of one or more metal atoms and their attendant oxygen atoms from a larger species to form *lacunary* derivatives. In some instances, this results in positional isomerism where the derivatives have identical charge, but *subtly* different geometry. These variations can modulate the reactivity of the isomeric species due to the different arrangement of the atoms. Remarkably, isomeric forms of $[PW_9O_{34}]^{9-}$, derived from 12-phosphotungstic acid, can be discriminated with a single protein nanopore.

The removal of three adjacent WO_6 fragments from the PTA structure[32] by hydrolytic cleavage of the M−O bonds results in a trivacant *lacunary* anion $[PW_9O_{34}]^{9-}$ where the central PO_4 tetrahedron is exposed either at its base (leading to the A-PW_9O_{34} type) or at its apex (leading to the B-PW_9O_{34} type) as shown schematically in Figure 4A. Heating a dry sample at 120 °C induces a solid-state isomerization from type A to type B, which is marked by a pronounced change in the IR phosphate stretching region ($1020-1200$ cm^{-1})[33] (Figure 4B). Although the structural differences between the two isomers are small, their reactivity toward divalent group VII metals (Zn^{2+}, Co^{2+}) is markedly different.[33b,34] The results in Figure 4C demonstrate that the αHL nanopore also discriminates between the two $Na_8HPW_9O_{34}$ isomers. Note that even though the two isomers were synthesized independently, both species are present, albeit at different concentrations[33b,34] due to isomerization in aqueous solution,[35] which happens for both isomers separately.

The blockade depth peaks for the type A and B species occur at $\langle i_A \rangle / \langle i_0 \rangle = 0.13 \pm 0.02$ and $\langle i_B \rangle / \langle i_0 \rangle = 0.08 \pm 0.01$, respectively. Because of the arrangement of the central PO_4 tetrahedron, the B-type PW_9 isomer has a smaller cavity compared to the A-type;[34] therefore, the B-type should have a larger volume. The B-type isomer is more effective at reducing the pore current, which suggests a blockade mechanism consistent with volume exclusion. Moreover, if the POMs had no chemical or physical interactions with the pore wall, they would only spend ~100 ns there (assuming it electrodiffuses the length of the pore, far too short a time to be detected with a conventional patch clamp amplifier).[27a] Thus, the vast majority of the time a given molecule spends in the pore is a consequence of the interaction between it and the pore wall. Considering $[PW_9O_{34}]^{9-}$ isomers have different reactivity, each could have different interactions with amino acid residues on the pore wall and therefore possibly be discriminated by both the blockade depth ratio and residence time. This is further supported by Figure 4D, which shows that the mean residence times for the two species differ by nearly a factor of 2: (117 ± 2) μs and (65 ± 1) μs, for Type A and Type B, respectively. The mean residence times were estimated from a least-squares fit of a single exponential function to the data corresponding to each species identified in Figure 4C (from a two Gaussian mixture model).

In summary, single-molecule measurements with a protein nanopore were used to investigate the 12-phosphotungstic acid derivatives induced by pH changes and to easily discriminate between the two isomers of the trivacant phosphotungstic acid in aqueous solution. Moreover, this new method allows simultaneous determination of multiple species in solution with greater sensitivity than conventional methods. The results suggest that nanopore-based analysis can serve as a complementary approach to traditional analytical chemistry tools in the study of

polyoxometalates. Other molecular properties with controlled geometrical changes, such as the different location of a given atom or a rotation of a fragment within the molecule, could potentially be investigated with this method. This technique opens further possibilities in the detailed characterization of metallic clusters.

■ ASSOCIATED CONTENT

ⓢ Supporting Information

The Supporting Information is available free of charge on the ACS Publications website at DOI: 10.1021/jacs.6b02917.

> Full experimental details and additional spectra and characterizations (PDF)

■ AUTHOR INFORMATION

Corresponding Author

*jessica.benjamini@nist.gov, jb3879@columbia.edu

Notes

The authors declare no competing financial interest.

■ ACKNOWLEDGMENTS

■ REFERENCES

(1) Bezrukov, S.; Kasianowicz, J. *Phys. Rev. Lett.* **1993**, *70* (15), 2352–2355.

(2) Kasianowicz, J. J.; Brandin, E.; Branton, D.; Deamer, D. W. *Proc. Natl. Acad. Sci. U. S. A.* **1996**, *93* (24), 13770–13773.

(3) Jin, Q.; Fleming, A. M.; Burrows, C. J.; White, H. S. *J. Am. Chem. Soc.* **2012**, *134* (26), 11006–11011.

(4) (a) Angevine, C. E.; Chavis, A. E.; Kothalawala, N.; Dass, A.; Reiner, J. E. *Anal. Chem.* **2014**, *86* (22), 11077–11085. (b) Astier, Y.; Uzun, O.; Stellacci, F. *Small* **2009**, *5* (11), 1273–1278. (c) Chavis, A. E.; Brady, K. T.; Kothalawala, N.; Reiner, J. E. *Analyst* **2015**, *140* (22), 7718–7725. (d) Campos, E.; McVey, C. E.; Carney, R. P.; Stellacci, F.; Astier, Y.; Yates, J. *Anal. Chem.* **2013**, *85* (21), 10149–10158. (e) Campos, E.; Asandei, A.; McVey, C. E.; Dias, J. C.; Oliveira, A. S. F.; Soares, C. M.; Luchian, T.; Astier, Y. *Langmuir* **2012**, *28* (44), 15643–15650.

(5) (a) Reiner, J. E.; Kasianowicz, J. J.; Nablo, B. J.; Robertson, J. W. F. *Proc. Natl. Acad. Sci. U. S. A.* **2010**, *107* (27), 12080–12085. (b) Baaken, G.; Halimeh, I.; Bacri, L.; Pelta, J.; Oukhaled, A.; Behrends, J. C. *ACS Nano* **2015**, *9* (6), 6443–6449. (c) Robertson, J. W. F. J.; Rodrigues, C. G. C.; Stanford, V. M. V.; Rubinson, K. A.; Krasilnikov, O. V.; Kasianowicz, J. J. *Proc. Natl. Acad. Sci. U. S. A.* **2007**, *104* (20), 8207–8211.

(6) Kang, X.-F.; Cheley, S.; Guan, X.; Bayley, H. *J. Am. Chem. Soc.* **2006**, *128* (33), 10684–10685.

(7) Halverson, K. M.; Panchal, R. G.; Nguyen, T. L.; Gussio, R.; Little, S. F.; Misakian, M.; Bavari, S.; Kasianowicz, J. J. *J. Biol. Chem.* **2005**, *280* (40), 34056–34062.

(8) Oukhaled, G.; Mathé, J.; Biance, A. L.; Bacri, L.; Betton, J. M.; Lairez, D.; Pelta, J.; Auvray, L. *Phys. Rev. Lett.* **2007**, *98* (15), 158101.

(9) Menestrina, G. *J. Membr. Biol.* **1986**, *90* (2), 177–190.

(10) Berzelius, J. J. *Ann. Phys.* **1826**, *82* (1), 369–392.

(11) Pope, M. T., Muller, A. M., Eds. *Polyoxometalates: From Platonic Solids to Anti-Retroviral Activity*; Springer Science & Business Media, 1994.

(12) Keita, B.; Nadjo, L. *J. Mol. Catal. A: Chem.* **2007**, *262* (1–2), 190–215.

(13) He, T.; Yao, J. *Prog. Mater. Sci.* **2006**, *51* (6), 810–879.

(14) Clemente-Juan, J. M.; Coronado, E. *Coord. Chem. Rev.* **1999**, *193–195*, 361–394.

(15) Donoeva, B. G.; Trubitsina, T. A.; Maksimov, G. M.; Maksimovskaya, R. I.; Kholdeeva, O. A. *Eur. J. Inorg. Chem.* **2009**, *2009* (34), 5142–5147.

(16) (a) Proust, A.; Thouvenot, R.; Gouzerh, P. *Chem. Commun.* **2008**, (16) 1837–1852. (b) Long, D.-L.; Tsunashima, R.; Cronin, L. *Angew. Chem., Int. Ed.* **2010**, *49* (10), 1736–1758. (c) Wang, Y.; Weinstock, I. A. *Chem. Soc. Rev.* **2012**, *41* (22), 7479–7496.

(17) Rhule, J. T.; Hill, C. L.; Judd, D. A. *Chem. Rev.* **1998**, *98* (1), 327–358.

(18) (a) Pu, F. F.; Wang, E. E.; Jiang, H. H.; Ren, J. J. *Mol. BioSyst.* **2013**, *9* (1), 113–120. (b) Yamase, T. *Mol. Eng.* **1993**, *3* (1–3), 241–262.

(19) Torrence, P. F. *Combating the Threat of Pandemic Influenza: Drug Discovery Approaches*; Wiley, 2007.

(20) Pope, M. T. *Heteropoly and Isopoly Oxometalates*; Springer-Verlag: Berlin Heidelberg, 1983; Vol. 8.

(21) Massart, R.; Contant, R.; Fruchart, J. M.; Ciabrini, J. P.; Fournier, M. *Inorg. Chem.* **1977**, *16* (11), 2916–2921.

(22) Keggins, $XM_{12}O_{40}{}^{q-}$ are composed of one heteroatom (X) surrounded by four oxygens to form a tetrahedron. The heteroatom is located centrally and caged by 12 octahedral MO_6 units (M = transition metal in their high oxidation state) linked to one another by the neighboring oxygen atoms.

(23) Reiner, J. E.; Balijepalli, A.; Robertson, J. W. F.; Campbell, J.; Suehle, J.; Kasianowicz, J. J. *Chem. Rev.* **2012**, *112* (12), 6431–6451.

(24) For example, the capture rates of POMs in cationic TRIS and citric acid-buffered solutions are significantly lower than a POM solution in a phosphate buffer (data not shown), presumably because the two buffers form a complex with the POM that do not partition into the pore.

(25) (a) Maksimovskaya, R. I. *Russ. J. Inorg. Chem.* **1998**, *43* (12), 1825–1837. (b) Fedotov, M. A.; Maksimovskaya, R. I. *J. Struct. Chem.* **2006**, *47* (5), 952–978.

(26) (a) Henrickson, S. E.; Misakian, M.; Robertson, B.; Kasianowicz, J. J. *Phys. Rev. Lett.* **2000**, *85* (14), 3057–3060. (b) Berg, H; Purcell, E. *Biophys. J.* **1977**, *20* (2), 193.

(27) Kasianowicz, J. J.; Robertson, J. W. F.; Chan, E. R.; Reiner, J. E.; Stanford, V. M. *Annu. Rev. Anal. Chem.* **2008**, *1* (1), 737–766.

(28) (a) Balijepalli, A.; Ettedgui, J.; Cornio, A. T.; Robertson, J. W. F.; Cheung, K. P.; Kasianowicz, J. J.; Vaz, C. *ACS Nano* **2014**, *8* (2), 1547–1553. (b) Balijepalli, A.; Robertson, J. W. F.; Reiner, J. E.; Kasianowicz, J. J.; Pastor, R. W. *J. Am. Chem. Soc.* **2013**, *135* (18), 7064–7072. (c) https://github.com/usnistgov/mosaic.

(29) (a) Knoth, W. H.; Harlow, R. L. *J. Am. Chem. Soc.* **1981**, *103* (7), 1865–1867. (b) Fuchs, J.; Thiele, A.; Palm, R. *Z. Naturforsch., B: J. Chem. Sci.* **1981**, *36b*, 544–550.

(30) Robertson, J. W. F.; Kasianowicz, J. J.; Reiner, J. E. *J. Phys.: Condens. Matter* **2010**, *22* (45), 454108.

(31) Kasianowicz, J. J.; Bezrukov, S. M. *Biophys. J.* **1995**, *69* (1), 94–105.

(32) Contant, R.; Fruchart, J. M.; Hervé, G.; Teze, A. *C. R. Seances Acad. Sci. Ser. C* **1974**, 1–7.

(33) (a) Finke, R. G.; Droege, M. W. *Inorg. Chem.* **1983**, *22* (6), 1006–1008. (b) Finke, R. G.; Droege, M. W.; Domaille, P. J. *Inorg. Chem.* **1987**, *26* (23), 3886–3896. (c) Domaille, P. J.; Hervé, G.; Taza, A. In *Inorganic Syntheses*; John Wiley & Sons, Inc.: Hoboken, NJ, 1990; Vol. 27, pp 96–104.

(34) Knoth, W. H.; Domaille, P. J.; Farlee, R. D. *Organometallics* **1985**, *4* (1), 62–68.

(35) Moore, B.; Foger, K. *Inorg. Chim. Acta* **1991**, *181*, 201–205.